FERMILAB-PUB-23-004-ND

First double-differential measurement of kinematic imbalance in neutrino interactions with the MicroBooNE detector

P. Abratenko,[35] O. Alterkait,[35] D. Andrade Aldana,[15] J. Anthony,[5] L. Arellano,[20] J. Asaadi,[34] A. Ashkenazi,[32]
S. Balasubramanian,[12] B. Baller,[12] G. Barr,[25] J. Barrow,[21,32] V. Basque,[12] O. Benevides Rodrigues,[31]
S. Berkman,[12] A. Bhanderi,[20] M. Bhattacharya,[12] M. Bishai,[3] A. Blake,[17] B. Bogart,[22] T. Bolton,[16] J. Y. Book,[14]
L. Camilleri,[10] D. Caratelli,[4] I. Caro Terrazas,[9] F. Cavanna,[12] G. Cerati,[12] Y. Chen,[28] J. M. Conrad,[21]
M. Convery,[28] L. Cooper-Troendle,[39] J. I. Crespo-Anadón,[6] M. Del Tutto,[12] S. R. Dennis,[5] P. Detje,[5] A. Devitt,[17]
R. Diurba,[2] Z. Djurcic,[1] R. Dorrill,[15] K. Duffy,[25] S. Dytman,[26] B. Eberly,[30] A. Ereditato,[2] J. J. Evans,[20]
R. Fine,[18] O. G. Finnerud,[20] W. Foreman,[15] B. T. Fleming,[39] N. Foppiani,[14] D. Franco,[39] A. P. Furmanski,[23]
D. Garcia-Gamez,[13] S. Gardiner,[12] G. Ge,[10] S. Gollapinni,[33,18] O. Goodwin,[20] E. Gramellini,[12] P. Green,[20,25]
H. Greenlee,[12] W. Gu,[3] R. Guenette,[20] P. Guzowski,[20] L. Hagaman,[39] O. Hen,[21] R. Hicks,[18] C. Hilgenberg,[23]
G. A. Horton-Smith,[16] B. Irwin,[23] R. Itay,[28] C. James,[12] X. Ji,[3] L. Jiang,[37] J. H. Jo,[3,39] R. A. Johnson,[8]
Y.-J. Jwa,[10] D. Kalra,[10] N. Kamp,[21] G. Karagiorgi,[10] W. Ketchum,[12] M. Kirby,[12] T. Kobilarcik,[12] I. Kreslo,[2]
M. B. Leibovitch,[4] I. Lepetic,[27] J.-Y. Li,[11] K. Li,[39] Y. Li,[3] K. Lin,[27] B. R. Littlejohn,[15] W. C. Louis,[18]
X. Luo,[4] C. Mariani,[37] D. Marsden,[20] J. Marshall,[38] N. Martinez,[16] D. A. Martinez Caicedo,[29] K. Mason,[35]
A. Mastbaum,[27] N. McConkey,[20,36] V. Meddage,[16] K. Miller,[7] J. Mills,[35] A. Mogan,[9] T. Mohayai,[12]
M. Mooney,[9] A. F. Moor,[5] C. D. Moore,[12] L. Mora Lepin,[20] J. Mousseau,[22] S. Mulleriababu,[2] D. Naples,[26]
A. Navrer-Agasson,[20] N. Nayak,[3] M. Nebot-Guinot,[11] J. Nowak,[17] N. Oza,[10,18] O. Palamara,[12] N. Pallat,[23]
V. Paolone,[26] A. Papadopoulou,[1,21] V. Papavassiliou,[24] H. B. Parkinson,[11] S. F. Pate,[24] N. Patel,[17] Z. Pavlovic,[12]
E. Piasetzky,[32] I. D. Ponce-Pinto,[39] I. Pophale,[17] S. Prince,[14] X. Qian,[3] J. L. Raaf,[12] V. Radeka,[3] A. Rafique,[1]
M. Reggiani-Guzzo,[20] L. Ren,[24] L. Rochester,[28] J. Rodriguez Rondon,[29] M. Rosenberg,[35] M. Ross-Lonergan,[18]
C. Rudolf von Rohr,[2] G. Scanavini,[39] D. W. Schmitz,[7] A. Schukraft,[12] W. Seligman,[10] M. H. Shaevitz,[10]
R. Sharankova,[12] J. Shi,[5] E. L. Snider,[12] M. Soderberg,[31] S. Söldner-Rembold,[20] J. Spitz,[22] M. Stancari,[12]
J. St. John,[12] T. Strauss,[12] S. Sword-Fehlberg,[24] A. M. Szelc,[11] W. Tang,[33] N. Taniuchi,[5] K. Terao,[28] C. Thorpe,[17]
D. Torbunov,[3] D. Totani,[4] M. Toups,[12] Y.-T. Tsai,[28] J. Tyler,[16] M. A. Uchida,[5] T. Usher,[28] B. Viren,[3] M. Weber,[2]
H. Wei,[19] A. J. White,[39] Z. Williams,[34] S. Wolbers,[12] T. Wongjirad,[35] M. Wospakrik,[12] K. Wresilo,[5] N. Wright,[21]
W. Wu,[12] E. Yandel,[4] T. Yang,[12] L. E. Yates,[12] H. W. Yu,[3] G. P. Zeller,[12] J. Zennamo,[12] and C. Zhang[3]
(The MicroBooNE Collaboration)[*]

[1] *Argonne National Laboratory (ANL), Lemont, IL, 60439, USA*
[2] *Universität Bern, Bern CH-3012, Switzerland*
[3] *Brookhaven National Laboratory (BNL), Upton, NY, 11973, USA*
[4] *University of California, Santa Barbara, CA, 93106, USA*
[5] *University of Cambridge, Cambridge CB3 0HE, United Kingdom*
[6] *Centro de Investigaciones Energéticas, Medioambientales y Tecnológicas (CIEMAT), Madrid E-28040, Spain*
[7] *University of Chicago, Chicago, IL, 60637, USA*
[8] *University of Cincinnati, Cincinnati, OH, 45221, USA*
[9] *Colorado State University, Fort Collins, CO, 80523, USA*
[10] *Columbia University, New York, NY, 10027, USA*
[11] *University of Edinburgh, Edinburgh EH9 3FD, United Kingdom*
[12] *Fermi National Accelerator Laboratory (FNAL), Batavia, IL 60510, USA*
[13] *Universidad de Granada, Granada E-18071, Spain*
[14] *Harvard University, Cambridge, MA 02138, USA*
[15] *Illinois Institute of Technology (IIT), Chicago, IL 60616, USA*
[16] *Kansas State University (KSU), Manhattan, KS, 66506, USA*
[17] *Lancaster University, Lancaster LA1 4YW, United Kingdom*
[18] *Los Alamos National Laboratory (LANL), Los Alamos, NM, 87545, USA*
[19] *Louisiana State University, Baton Rouge, LA, 70803, USA*
[20] *The University of Manchester, Manchester M13 9PL, United Kingdom*
[21] *Massachusetts Institute of Technology (MIT), Cambridge, MA, 02139, USA*
[22] *University of Michigan, Ann Arbor, MI, 48109, USA*
[23] *University of Minnesota, Minneapolis, MN, 55455, USA*
[24] *New Mexico State University (NMSU), Las Cruces, NM, 88003, USA*
[25] *University of Oxford, Oxford OX1 3RH, United Kingdom*
[26] *University of Pittsburgh, Pittsburgh, PA, 15260, USA*
[27] *Rutgers University, Piscataway, NJ, 08854, USA*

[28]SLAC National Accelerator Laboratory, Menlo Park, CA, 94025, USA
[29]South Dakota School of Mines and Technology (SDSMT), Rapid City, SD, 57701, USA
[30]University of Southern Maine, Portland, ME, 04104, USA
[31]Syracuse University, Syracuse, NY, 13244, USA
[32]Tel Aviv University, Tel Aviv, Israel, 69978
[33]University of Tennessee, Knoxville, TN, 37996, USA
[34]University of Texas, Arlington, TX, 76019, USA
[35]Tufts University, Medford, MA, 02155, USA
[36]University College London, London WC1E 6BT, United Kingdom
[37]Center for Neutrino Physics, Virginia Tech, Blacksburg, VA, 24061, USA
[38]University of Warwick, Coventry CV4 7AL, United Kingdom
[39]Wright Laboratory, Department of Physics, Yale University, New Haven, CT, 06520, USA

(Dated: January 9, 2023)

We report the first measurement of flux-integrated double-differential quasielastic-like neutrino-argon cross sections, which have been made using the Booster Neutrino Beam and the MicroBooNE detector at Fermi National Accelerator Laboratory. The data are presented as a function of kinematic imbalance variables which are sensitive to nuclear ground state distributions and hadronic reinteraction processes. We find that the measured cross sections in different phase-space regions are sensitive to different nuclear effects. Therefore, they enable the impact of specific nuclear effects on the neutrino-nucleus interaction to be isolated more completely than was possible using previous single-differential cross section measurements. Our results provide precision data to help test and improve neutrino-nucleus interaction models. They further support ongoing neutrino-oscillation studies by establishing phase-space regions where precise reaction modeling has already been achieved.

Neutrino oscillation measurements aim to extract neutrino mixing angles, mass differences, and the charge-parity violating phase, and to search for new physics beyond the Standard Model [1–3]. The analysis of such measurements traditionally relies on detailed comparisons of measured and theoretically-expected neutrino interaction rates in the corresponding detectors. Therefore, a precise understanding of neutrino-nucleus interactions is required to fully exploit the discovery potential of current and next-generation experiments.

With a growing number of neutrino-oscillation experiments employing liquid argon time projection chamber (LArTPC) neutrino detectors [4–9], high-accuracy modeling of neutrino-argon interactions is becoming of paramount importance [10–12]. The overarching goal of these efforts is both to achieve few-percent-level modeling of neutrino-argon interaction rates and to provide a detailed understanding of the final-state kinematics of emitted particles that are used to reconstruct the energies of the interacting neutrinos [13, 14].

This Letter reports the first measurement of flux-integrated double-differential cross sections for muon-neutrino-argon (ν_μ-Ar) charged-current (CC) quasielastic (QE)-like scattering reactions as a function of transverse kinematic imbalance variables. Building upon a previous analysis of neutrino-argon cross sections with a similar signal event topology [15], we focus on reactions where the neutrino removes a single intact proton from the nucleus without producing any additional detected particles. The results reported here are obtained using the Booster Neutrino Beam (BNB) and the MicroBooNE detector at Fermi National Accelerator Laboratory with an exposure of 6.79×10^{20} protons on target.

Transverse kinematic imbalance variables were previously shown to be sensitive to the modeling of the nuclear ground-state distribution and to nuclear medium effects, such as hadronic final-state interactions (FSI) [16–21]. By measuring the components of the muon and proton momenta perpendicular to the neutrino direction, $\vec{p}_T^{\,\mu}$ and $\vec{p}_T^{\,p}$ respectively, we construct the transverse missing momentum, $\delta\vec{p}_T = \vec{p}_T^{\,\mu} + \vec{p}_T^{\,p}$, and its angular orientation with respect to $\vec{p}_T^{\,\mu}$, $\delta\alpha_T = \arccos\left(\frac{-\vec{p}_T^{\,\mu}\cdot\delta\vec{p}_T}{p_T^{\,\mu}\,\delta p_T}\right)$. Due to the isotropic nature of Fermi motion, $\delta\alpha_T$ is expected to be uniformly distributed in the absence of any FSI. In the presence of FSI, the proton momentum is generally reduced and the $\delta\alpha_T$ distribution becomes enhanced towards 180°. Similarly, the shape of the δp_T distribution encapsulates information related to Fermi motion and is further smeared due to FSI and multi-nucleon effects. Given the sensitivity of $\delta\alpha_T$ to FSI and of δp_T to both FSI and Fermi motion, a simultaneous measurement of these two observables can help to disentangle the individual impact of each nuclear effect on the neutrino-nucleus interaction. Similarly, the muon-proton momentum imbalance components transverse and parallel to the transverse lepton momentum, $\delta p_{T,x} = \delta p_T \cdot \sin\delta\alpha_T$ and $\delta p_{T,y} = \delta p_T \cdot \cos\delta\alpha_T$, provide further handles on Fermi motion and FSI processes, respectively.

The active volume of the MicroBooNE LArTPC contains 85 tonnes of argon [22]. It is exposed to the BNB neutrino energy spectrum that peaks around 0.8 GeV and extends to about 2 GeV.

Neutrinos are detected by measuring the charged particles produced following their interactions with argon

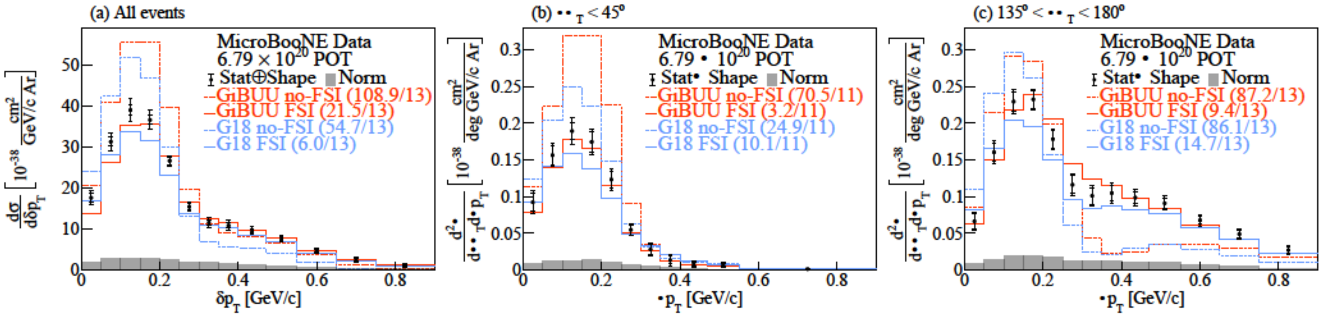

FIG. 1. The flux-integrated (a) single- and (b-c) double- (in $\delta\alpha_T$ bins) differential CC1p0π cross sections as a function of the transverse missing momentum δp_T. Inner and outer error bars show the statistical and total (statistical and shape systematic) uncertainty at the 1σ, or 68%, confidence level. The gray band shows the separate normalization systematic uncertainty. Colored lines show the results of theoretical cross section calculations with (solid line) and without (dashed line) FSI based on the `GENIE` (blue) and **GiBUU** (orange) event generators.

nuclei in the LArTPC active volume. These charged particles travel through the liquid argon, producing both scintillation light and trails of ionization electrons. In the presence of a uniform 273 V/cm electric field, the ionization electrons drift through the argon and are detected by a system of three anode wire planes that are perpendicular to the field. The scintillation light is measured by photomultiplier tubes (PMTs). Events are recorded if the PMT signals are in time coincidence with the beam arrival time. Trigger hardware and software selection cuts reject background events, mostly from cosmic muons, providing enriched data samples in which a neutrino interaction occurs in ≈ 15% of selected beam spills [23].

The **Pandora** reconstruction package [24] is used to form individual tracks from the measured ionization signals in the enriched data samples. Particle identification and momentum determination are performed using the measured track energy-deposition profile and track length [25, 26].

Candidate muon-proton pairs are identified by requiring exactly two track-like objects and no shower-like objects based on a track-score variable from **Pandora** [27, 28]. The discriminant described in [29] is used to distinguish muon and proton candidates. We further apply quality cuts to avoid mis-reconstructed tracks. Details are given in [30].

To reduce contributions from cosmic tracks and to minimize bin-migration effects, the event selection considers only muon and proton track pairs that are fully contained within a fiducial volume of 10 cm from the edge of the detector active volume.

The signal definition used in this analysis includes all ν_μ-Ar scattering events with a final-state muon with momentum $0.1 < p_\mu < 1.2$ GeV/c and exactly one final-state proton with $0.3 < p_p < 1$ GeV/c. Events with final-state neutral pions at any momentum are excluded. Signal events may contain additional protons with momentum less than 300 MeV/c or greater than 1 GeV/c, neutrons at any momentum, and charged pions with momentum lower than 70 MeV/c. We refer to the signal events as CC1p0π.

After the application of the event selection, we retain 9051 data events that satisfy all criteria. Event distributions for all the aforementioned variables of interest and details on the CC1p0π event selection can be found in [30].

The flux-averaged differential event rate as a function of a given variable x in bin i is obtained by

$$\frac{dR}{dx_i} = \frac{N_i - B_i}{T \cdot \Phi_\nu \cdot \Delta_i} \tag{1}$$

where N_i and B_i are the number of measured events and the expected background events, respectively. T is the number of target argon nuclei in the fiducial volume of interest. Φ_ν corresponds to the total BNB flux and, finally, Δ_i corresponds to the i-th bin width or area for the single- and double-differential results, respectively.

We report the extracted cross sections for the measured interaction using the Wiener singular value decomposition (Wiener-SVD) unfolding technique as a function of unfolded kinematic variables [31]. More details on the unfolding procedure can be found in [30]. The unfolding machinery returns the unfolded differential cross section and the corresponding uncertainties. Apart from the unfolded result, an additional smearing matrix A_C is obtained, which accounts for the regularization and bias of the measurement. When a comparison to the unfolded data is performed, the corresponding A_C matrices must be applied to the true cross section predictions. See Supplemental Material for the data release, the unfolded covariance matrices, and the additional matrices A_C.

As in previous MicroBooNE measurements [15, 32–34], the full Monte Carlo (MC) simulation used in the unfolding procedure consists of a combination of simulated neutrino interactions overlaid on beam-off background events. This provides an accurate description of the dominant cosmic backgrounds pertinent to surface detectors

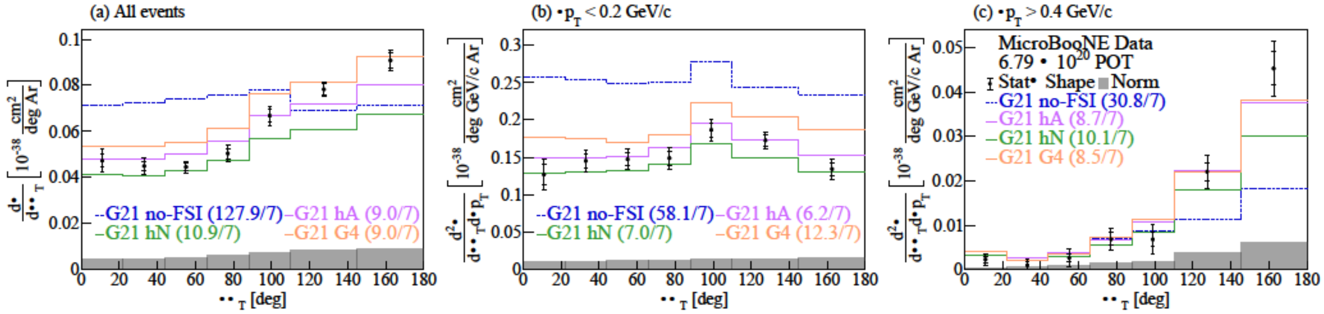

FIG. 2. The flux-integrated (a) single- and (b-c) double- (in δp_T bins) differential CC1p0π cross sections as a function of the angle $\delta\alpha_T$. Inner and outer error bars show the statistical and total (statistical and shape systematic) uncertainty at the 1σ, or 68%, confidence level. The gray band shows the separate normalization systematic uncertainty. Colored lines show the results of theoretical cross section calculations with a number of FSI-modeling choices based on the `GENIE` event generator.

using real data. Neutrino interactions are simulated using the `GENIE v3.0.6` event generator [35, 36], where the CC QE and CC meson exchange current (MEC) neutrino interaction models have been tuned to T2K ν_μ-^{12}C CC0π data [37, 38]. We refer to the corresponding prediction as `G18`. `GENIE` generates all final-state particles associated with the primary neutrino interaction and propagates them through the nucleus, accounting for FSI. The particle propagation outside the nucleus is simulated using `GEANT4` [39], with the MicroBooNE detector response modeled using the `LArSoft` framework [40, 41]. Based on this simulation, we estimate that our efficiency for selecting CC1p0π events is $\approx$ 10%, with a purity of $\approx$ 70%.

The total covariance matrix $E = E^{\mathrm{stat}} + E^{\mathrm{syst}}$ used in the Wiener-SVD filter includes the statistical and systematic uncertainties associated with our measurement. E^{stat} is a diagonal covariance matrix including the statistical uncertainties and E^{syst} is a covariance matrix incorporating the total systematic uncertainties. More details on the construction of these matrices can be found in [30]. These matrices include uncertainties on the integrated cross section due to the neutrino flux prediction (7.3%), neutrino interaction cross section modeling (5.3%), detector response modeling (4.9%), beam exposure (2.3%), statistics (1.5%), number-of-scattering-targets (1.15%), reinteractions (1%), and out-of-cryostat interaction modeling (0.2%). The full fractional uncertainty on the integrated total cross section sums to 11%.

Across the results reported in this Letter, statistical uncertainties are shown by the inner error bars on the final results. The systematic uncertainties were decomposed into shape- and normalization-related sources following the procedure outlined in [42]. The cross-term uncertainties were incorporated in the normalization part. The outer error bars on the reported cross sections correspond to statistical and shape uncertainties added in quadrature. The normalization uncertainties are presented with the gray band at the bottom of our results.

The single- and double-differential results as a function of δp_T are presented in Fig. 1. They are compared with `G18` and the theory-driven `GiBUU 2021 (GiB)` event generator. Additional comparisons to the corresponding event generators when FSI are turned off are also included (`G18 no-FSI` and `GiBUU no-FSI`). `G18` uses the local Fermi gas (LFG) model of the nuclear ground state [43] and the Nieves CCQE scattering prescription [44] with Coulomb corrections for the outgoing muon [45] and random phase approximation (RPA) corrections [46]. It also uses the Nieves MEC model [47], the KLN-BS resonance (RES) [48–51] and Berger-Sehgal coherent (COH) [52] scattering models. Furthermore, the hA2018 FSI model [53] and the MicroBooNE-specific tuning of model parameters [38] are utilized. `GiBUU` uses somewhat similar models, but, unlike `GENIE`, they are implemented in a coherent way by solving the Boltzmann-Uehling-Uhlenbeck transport equation [54]. The simulation includes the LFG model [43], a standard CCQE expression [55], an empirical MEC model and a dedicated spin-dependent resonances amplitude calculation following the `MAID` analysis [54]. The deep inelastic (DIS) model is from `PYTHIA` [56]. The FSI treatment is different as the hadrons propagate through the residual nucleus in a nuclear potential which is consistent with the initial state.

The single-differential results as a function of δp_T using all the events that satisfy our selection are shown in Fig. 1a. The χ^2/bins data comparison for each generator shown on all the results takes into account the total covariance matrix, including the off-diagonal elements. Theoretical uncertainties on the models themselves are not included. The peak height of both generator predictions is $\approx$ 30% higher when FSI effects are turned off. Yet, all distributions illustrate a transverse missing momentum tail that extends beyond the Fermi momentum ($\approx 250\,\mathrm{MeV}/c$) whether FSI effects are incorporated or not. The double-differential result using events with $\delta\alpha_T < 45°$ shown in Fig. 1b is dominated by events that

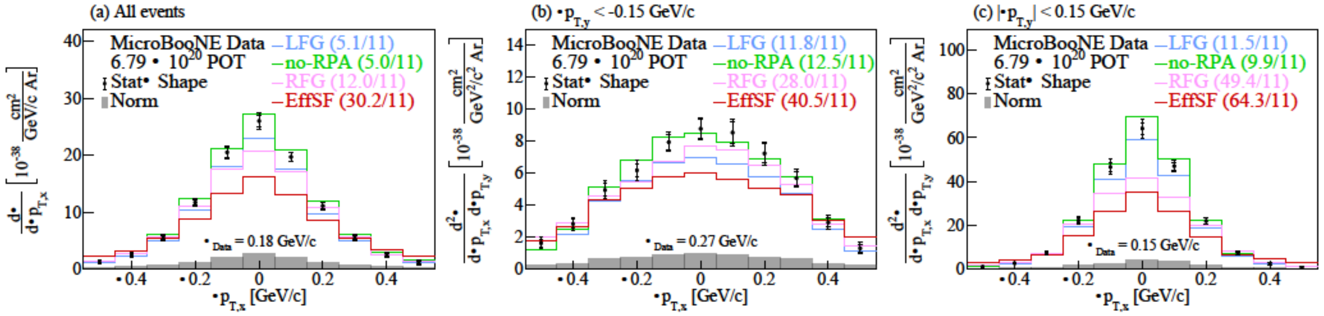

FIG. 3. The flux-integrated (a) single- and (b-c) double- (in $\delta p_{T,y}$ bins) differential CC1p0π cross sections as a function of the transverse three-momentum transfer component, $\delta p_{T,x}$. Inner and outer error bars show the statistical and total (statistical and shape systematic) uncertainty at the 1σ, or 68%, confidence level. The gray band shows the separate normalization systematic uncertainty. Colored lines show the results of theoretical cross section calculations with a number of event generators. The standard deviation (σ_{Data}) of a Gaussian fit to the data is shown on each panel.

primarily occupy the region up to the Fermi momentum and do not exhibit a high-momentum tail. The double-differential results using events with $135° < \delta\alpha_T < 180°$ are shown in Fig. 1c and illustrate high transverse missing momentum up to 1 GeV/c. The prediction without FSI effects is strongly disfavored. Therefore, the high δp_T region is an appealing candidate for neutrino experiments to benchmark and tune the FSI modeling in event generators.

Extracted cross sections as a function of $\delta\alpha_T$ are shown in Fig. 2. Here we perform comparisons to the recently added theory driven `GENIE v3.0.6 G21_11b_00_000` configuration (`G21 hN`) [57]. This configuration uses the SuSAv2 model for CCQE and CCMEC interactions [58], and the hN2018 FSI model [59]. The modeling choices for RES, DIS, and COH interactions are the same as for `G18`. We investigated the effect of the FSI-modeling choice by comparing the `G21 hN` results to the ones obtained with `G21 hA`, where the hA2018 FSI model was used instead, and to `G21 G4` with the recently coupled `GEANT4` FSI framework [60]. The prediction where the FSI effects have been turned off (`G21 no-FSI`) is also included for comparison.

The single-differential results as a function of $\delta\alpha_T$ using all the events that satisfy our selection are shown in Fig. 2a. The prediction without FSI shows a uniform behavior as a function of $\delta\alpha_T$ and is disfavored by the data. The addition of FSI effects leads to a $\approx 30\%$ asymmetry around $\delta\alpha_T = 90°$. The three FSI models used here for comparison yield a consistent behavior. The double-differential result shown in Fig. 2b using events with $\delta p_T < 0.2$ GeV/c illustrates a uniform distribution indicative of the suppressed FSI impact in that part of the phase-space. The `G21 no-FSI` prediction is higher than the other FSI predictions. The difference comes from the generation of multiple particles above detection threshold due to reinteraction effects in the FSI-rich samples. Such events do not satisfy the signal definition and therefore introduce the difference in the absolute scale. The double-differential results using events with $\delta p_T > 0.4$ GeV/c are shown in Fig. 2c and illustrate the presence of strong FSI effects with a significantly enhanced asymmetry around 90°. Thus, the high $\delta\alpha_T$ region is highly informative for the FSI-modeling performance in event generators. See Supplemental Material for details on the interaction breakdown of the aforementioned results and [30] for further double-differential results.

Finally, Fig. 3 shows the single- and double-differential results as a function of $\delta p_{T,x}$. The result shows the comparison between the nominal `G18` model using the local Fermi gas (`LFG`) and predictions using the same `G18` interaction processes but different nuclear ground-state model options available in the `GENIE` event generator, namely the Bodek-Ritchie Fermi Gas (`RFG`) [61] and an effective spectral function (`EffSF`) [62]. Furthermore, the prediction without RPA effects is shown for comparison (`no-RPA`) [46].

The single-differential result (Fig. 3a) illustrates a fairly broad symmetric distribution centered around 0 GeV/c. The double-differential result for events where $\delta p_{T,y} <$ -0.15 GeV/c (Fig. 3b) illustrates an even broader distribution, as can be seen in the widths (σ_{Data}) of Gaussian fits on the data distributions. Conversely, the double-differential result for events with $|\delta p_{T,y}| <$ 0.15 GeV/c (Fig. 3c) shows a much narrower peak which strongly depends on the choice of the underlying model and the inclusion or absence of nuclear effects such as RPA. The `LFG` and `no-RPA` predictions are favored in both parts of the phase-space. The Supplemental Material contains details on the interaction breakdown of various generator predictions for the results reported here, and further single- and double-differential results can be found in [30].

In summary, we report the first measurement of muon neutrino double-differential cross sections on argon as a function of kinematic imbalance variables for event topologies with a single muon and a single proton detected in the final state. We identify parts of the phase space where the Fermi motion can be largely disentangled from FSI and multi-nucleon effects. This disentanglement provides leverage to improve separate parts of the complicated neutrino interaction models that affect single-differential distributions in similar ways. Therefore, the reported results pave the path to substantially reducing cross section systematic uncertainties which will enable precision measurements of fundamental neutrino properties.

This document was prepared by the MicroBooNE collaboration using the resources of the Fermi National Accelerator Laboratory (Fermilab), a U.S. Department of Energy, Office of Science, HEP User Facility. Fermilab is managed by Fermi Research Alliance, LLC (FRA), acting under Contract No. DE-AC02-07CH11359. MicroBooNE is supported by the following: the U.S. Department of Energy, Office of Science, Offices of High Energy Physics and Nuclear Physics; the U.S. National Science Foundation; the Swiss National Science Foundation; the Science and Technology Facilities Council (STFC), part of the United Kingdom Research and Innovation; the Royal Society (United Kingdom); the UK Research and Innovation (UKRI) Future Leaders Fellowship; and The European Union's Horizon 2020 Marie Sklodowska-Curie Actions. Additional support for the laser calibration system and cosmic ray tagger was provided by the Albert Einstein Center for Fundamental Physics, Bern, Switzerland. We also acknowledge the contributions of technical and scientific staff to the design, construction, and operation of the MicroBooNE detector as well as the contributions of past collaborators to the development of MicroBooNE analyses, without whom this work would not have been possible. For the purpose of open access, the authors have applied a Creative Commons Attribution (CC BY) license to any Author Accepted Manuscript version arising from this submission.

---

[*] microboone_info@fnal.gov

[1] M. Tanabashi *et al.* (Particle Data Group), Phys. Rev. D **98**, 030001 (2018).
[2] K. Abe *et al.* (T2K Collaboration), Nature **580**, 339 (2020).
[3] M. A. Acero *et al.* (NOvA Collaboration), Phys. Rev. Lett. **123**, 151803 (2019).
[4] B. Abi *et al.* (DUNE Collaboration), arXiv (2018), 1807.10334 [physics.ins-det].
[5] B. Abi *et al.* (DUNE Collaboration), arXiv (2018), 1807.10327 [physics.ins-det].
[6] B. Abi *et al.* (DUNE Collaboration), arXiv (2018), 1807.10340 [physics.ins-det].
[7] M. Antonello *et al.* (MicroBooNE, LAr1-ND, ICARUS-WA104), arXiv (2015), 1503.01520 [physics.ins-det].
[8] F. Tortorici, V. Bellini, and C. Sutera (ICARUS Collaboration), J. Phys. Conf. Ser. **1056**, 012057 (2018).
[9] B. Abi *et al.* (DUNE Collaboration), arXiv (2018), 1807.10334 [physics.ins-det].
[10] S. Dolan, U. Mosel, K. Gallmeister, L. Pickering, and S. Bolognesi, Phys. Rev. C **98**, 045502 (2018).
[11] N. Rocco, A. Lovato, and O. Benhar, Phys. Rev. Lett. **116**, 192501 (2016).
[12] N. Rocco, Frontiers in Physics **8**, 116 (2020).
[13] K. Abe *et al.* (Hyper-Kamiokande Collaboration), arXiv (2018), 1805.04163 [physics.ins-det].
[14] B. Abi *et al.* (DUNE Collaboration), arXiv (2020), 2002.03005 [hep-ex].
[15] P. Abratenko *et al.* (MicroBooNE Collaboration), Phys. Rev. Lett. **125**, 201803 (2020).
[16] A. Bodek and T. Cai, Eur. Phys. J. C **79**, 293 (2019).
[17] X.-G. Lu, L. Pickering, S. Dolan, G. Barr, D. Coplowe, Y. Uchida, D. Wark, M. O. Wascko, A. Weber, and T. Yuan, Phys. Rev. C **94**, 015503 (2016).
[18] K. Abe *et al.* (T2K Collaboration), Phys. Rev. D **98**, 032003 (2018).
[19] X.-G. Lu *et al.* (MINERvA Collaboration), Phys. Rev. Lett. **121**, 022504 (2018).
[20] T. Cai *et al.* (MINERvA Collaboration), Phys. Rev. D **101**, 092001 (2020).
[21] L. Bathe-Peters, S. Gardiner, and R. Guenette, arXiv (2022), 2201.04664 [hep-ph].
[22] R. Acciarri *et al.* (MicroBooNE Collaboration), J. Instrum. **12**, P02017 (2017).
[23] D. Kaleko, J. Instrum. **8**, C09009 (2013).
[24] R. Acciarri *et al.* (MicroBooNE Collaboration), Eur. Phys. J. C **78**, 82 (2018).
[25] "Table 289: Muons in liquid argon (Ar)," `http://pdg.lbl.gov/2012/AtomicNuclearProperties/MUON_ELOSS_TABLES/muonloss_289.pdf` (2012).
[26] S. K. H. Bichsel, D. E. Groom, "Passage of particles through matter," PDG Chapter 27, Figure 27.1 `http://pdg.lbl.gov/2005/reviews/passagerpp.pdf` (2005).
[27] W. Van De Pontseele, *Search for Electron Neutrino Anomalies with the MicroBooNE Detector*, Ph.D. thesis, Oxford U. (2020).
[28] P. Abratenko *et al.* (MicroBooNE Collaboration), Phys. Rev. D **105**, 112004 (2022).
[29] P. Abratenko *et al.* (MicroBooNE Collaboration), J. High Energ. Phys. **2021**, 153 (2021).
[30] P. Abratenko *et al.* (MicroBooNE Collaboration), arXiv (2022), 4684375 [hep-ex].
[31] W. Tang, X. Li, X. Qian, H. Wei, and C. Zhang, J. Instrum. **12**, P10002–P10002 (2017).
[32] C. Adams *et al.* (MicroBooNE Collaboration), Eur. Phys. J. C **79**, 673 (2019).
[33] P. Abratenko *et al.* (MicroBooNE Collaboration), Phys. Rev. Lett. **128**, 151801 (2022).
[34] P. Abratenko *et al.* (MicroBooNE Collaboration), Phys. Rev. D **105**, L051102 (2022).
[35] C. Andreopoulos *et al.*, Nucl. Instrum. Meth. A **614**, 87 (2010).
[36] C. Andreopoulos *et al.*, arXiv (2015), 1510.05494 [hep-ph].
[37] K. Abe *et al.* (T2K Collaboration), Phys. Rev. D **93**, 112012 (2016).
[38] P. Abratenko *et al.* (MicroBooNE Collaboration), Phys. Rev. D **105**, 072001 (2022).
[39] S. Agostinelli *et al.* (GEANT4), Nucl. Instrum. Meth. A **506**, 250 (2003).
[40] R. Pordes and E. Snider, PoS **ICHEP2016**, 182 (2016).
[41] E. Snider and G. Petrillo, J. Phys. Conf. Ser. **898**, 042057

(2017).

[42] K. Mahn, *A search for muon neutrino and antineutrino disappearance in the Booster Neutrino Beam*, Ph.D. thesis, Columbia University (2009).

[43] R. Carrasco and E. Oset, Nucl. Phys. A **536**, 445 (1992).

[44] J. Nieves, F. Sanchez, I. Ruiz Simo, and M. Vicente Vacas, Phys. Rev. D **85**, 113008 (2012).

[45] J. Engel, Phys. Rev. C **57**, 2004 (1998).

[46] J. Nieves, J. E. Amaro, and M. Valverde, Phys. Rev. C **70**, 055503 (2004).

[47] J. Schwehr, D. Cherdack, and R. Gran, arXiv (2016), 1601.02038 [hep-ph].

[48] J. A. Nowak (MiniBooNE Collaboration), AIP Conf. Proc. **1189**, 243 (2009).

[49] K. Kuzmin, V. Lyubushkin, and V. Naumov, Phys. Part. Nucl. **35**, S133 (2004).

[50] C. Berger and L. Sehgal, Phys. Rev. D **76**, 113004 (2007).

[51] K. M. Graczyk and J. T. Sobczyk, Phys. Rev. D **77**, 053001 (2008), [Erratum: Phys.Rev.D 79, 079903 (2009)].

[52] C. Berger and L. Sehgal, Phys. Rev. D **79**, 053003 (2009).

[53] D. Ashery, I. Navon, G. Azuelos, H. Walter, H. Pfeiffer, and F. Schleputz, Phys. Rev. C **23**, 2173 (1981).

[54] U. Mosel, Phys. Rev. G **46**, 113001 (2019).

[55] T. Leitner, L. Alvarez-Ruso, and U. Mosel, Phys. Rev. C **73**, 065502 (2006).

[56] T. Sjostrand, S. Mrenna, and P. Z. Skands, J. High Energ. Phys. **05**, 026 (2006).

[57] L. Alvarez-Ruso *et al.* (GENIE Collaboration), Eur. Phys. J. ST **230**, 4449 (2021).

[58] S. Dolan, G. D. Megias, and S. Bolognesi, Phys. Rev. D **101**, 033003 (2020).

[59] S. Dytman, Y. Hayato, R. Raboanary, J. T. Sobczyk, J. Tena-Vidal, and N. Vololoniaina, Phys. Rev. D **104**, 053006 (2021).

[60] D. H. Wright and M. H. Kelsey, Nucl. Instrum. Meth. A **804**, 175 (2015).

[61] A. Bodek and J. L. Ritchie, Phys. Rev. D **23**, 1070 (1981).

[62] A. M. Ankowski and J. T. Sobczyk, Phys. Rev. C **74**, 054316 (2006).